# A highly innovative yet cost-effective multi-generation energy system for net-zero energy buildings

Ahmad Arabkoohsar[1], Amirmohammad Behzadi[1,*], Natasa Nord[2]

[1]Department of Energy Technology, Aalborg University, Denmark

[2]Department of Energy and Process Engineering, Norwegian University of Science and Technology, Norway

*Corresponding Author: ambe@et.aau.dk

## Abstract

This study introduced an innovative yet feasible and cost-effective solution to make a big step forward in the state-of-art of smart energy buildings and obtain a real meaning of net-zero energy building. In this study, the main cornerstones of the developed solution combined the following technologies: the use of novel trigeneration solar collectors without a battery, a very clever method of heat pump integration with minimal size and cost required, and two-way interaction of the building with local energy networks. Different system configurations based on the included components were suggested and analyzed for an apartment building in Denmark. A thorough techno-economic and environmental evaluation of the proposed solution and the most competent ones already proposed for the same application was carried out to rank the best configuration from various facets. A comparative parametric study was accomplished to examine and compare the variation of performance indicators with significant decision variables. In addition, the tri-objective optimization was implemented for each configuration to specify the best optimum condition from energy, economic, and environmental standpoints. According to the economic results, the configurations integrated with battery and regular heat pumps were not favorable due to the highest total cost and the payback period. Here, the proposed system, owing to its resilient energy trade possibility with the energy networks and the scaled-down heat pump, gave larger energy-saving and $CO_2$ emission reduction rates of 16.6% and 21.6%, respectively. The multi-objective optimization showed that the capacities of the battery and the cold storage were the most effective parameters on the performance of the system.

**Keywords:** Net-zero energy building; Scaled-down heat pump; Building integrated PVT; Photovoltaic thermal cooling panels; Multi-objective optimization.

| **Nomenclature** | | | |
|---|---|---|---|
| *A* | Area, $m^2$ | *Subscripts and abbreviations* | |
| *AC* | The annual cost, $ | *V* | Volume, $m^3$ |

| | | | |
|---|---|---|---|
| $ACSR$ | Annual cost saving rate | $\dot{W}$ | Power, kWh |
| $C_P$ | Specific heat capacity, kJ/(kg.K) | $Z$ | Component cost |
| $C_{tot}$ | Total cost, $ | abs | Absorber |
| $CDE$ | Carbon dioxide emission, kg | amb | Ambient |
| $CDERR$ | Carbon dioxide emission reduction rate | CHP | Combined heating and power |
| $\dot{E}$ | Electricity, kWh | CCHP | Combined cooling, heating, and power |
| $F$ | Fuel consumption, kWh | CI | Capital investment |
| $G$ | Total incident solar radiation, kW/m$^2$ | Conv | Convection |
| $h$ | Enthalpy (kJ/kg) | i | Inlet |
| $h_{c,forced}$ | Forced convection heat transfer coefficient, W/(m$^2$K) | nat | natural |
| $h_{c,mix}$ | Mixed convection heat transfer coefficient, W/(m$^2$K) | OM | Operating and maintenance |
| $h_{c,nat}$ | Natural convection heat transfer coefficient, W/(m$^2$K) | o | Outlet |
| $\dot{m}$ | Mass flow rate, kg/s | PP | Payback period |
| $NPV$ | Net present value, $ | PV | Photovoltaic |
| $P$ | Pressure | PVT | Photovoltaic/Thermal |
| $PESR$ | Primary energy saving rate | PVTC | Photovoltaic/Thermal/Cooling |
| $PP$ | Payback period | rad | Radiation |
| $Q_{loss,top,conv}$ | The energy lost through convection at the top surface, kW | SP | Separation production |
| $Q_{loss,top,rad}$ | The energy lost through radiation at the top surface, kW | *Greek letters* | |
| $Q_{loss,back}$ | The energy lost at the back of the collector, kW | $\eta_E$ | Electrical efficiency of the CHP waste to the energy plant |
| $Q_{useful}$ | Energy added to the flow stream, kW | $\eta_{Grid}$ | Network's energy transmission efficiency |
| $R_B$ | The heat transfer resistance through the back of the PVT | $\eta_H$ | Heat efficiency of the CHP waste to the energy plant |
| $T$ | Temperature | $\eta_{PV}$ | PV efficiency |
| $U$ | loss coefficient between the tank and its environment, kJ/(kg.K.m$^2$) | $\varepsilon$ | Emissivity at the top of the panel |

## 1. Introduction

Today, the global renewable energy expansion and the international appropriate development objectives towards climate protection are central areas of scientific attention in the world, particularly in Europe [1]. The trend is expected to continue due to the rapid depletion of fossil fuels and a significant increase in energy use. More than 40% of the total $CO_2$ emission and nearly 33% of global energy use corresponds to the buildings sector [2]. Massive emission mitigation and efficiency improvement potentials of buildings remain untapped because of inadequate attention to sustainable buildings [3,4]. A smart energy system with a flexible and intelligent link between energy production, use, and distribution is a sustainable, cost-effective, and environmentally friendly solution to address the global issues regarding the buildings sector

[5]. The two important characteristics of smart buildings might be: 1) the use of renewable sources and 2) the two-way interaction of the building with the local grid making the building's net traded energy with the grids practically zero [6]. This way, a strong synergy between different renewable energy sources and higher collaborations between energy producers and users is promoted to achieve cleaner production and efficient integration. Among different sources, the utilization of solar energy and solar technologies based on the most advanced state-of-practice is of great importance for much higher penetration of renewable energy [7].

Solar photovoltaic (PV) and solar thermal panels in building energy systems are quite common. PV's main deficiency is decreasing efficiency as tits surface temperature picks up. The idea of photovoltaic thermal (PVT) panel has been developed to increase the electrical efficiency of the panel via a working fluid flow, decreasing its surface temperature and exploit the waste heat for heating applications [8]. A comparison between the PVT system and PV panel integrated with solar collector was carried out by Good et al. [9] to achieve a net-zero energy building for Norway's case. They concluded that the PVT system is superior from techno-economical facets despite the existing material challenges. A nearly zero-energy building supplied by PVT panel interacting with electricity grid was proposed by Conti et al. [10]. They showed that a higher share of renewable energy is achieved using PVT compared to side-by-side PV panels and thermal collectors. Tse et al. [11] conducted a techno-economic comparison and sensitive assessment of a nearly zero-energy/emission office building equipped with PVT panels and side-by-side PV-solar thermal collectors for the case of Hong Kong. They showed that the PVT-based model is superior because of higher performance efficiency and lower payback period than the PV-solar collector system. Wang et al. [12] assessed and compared the energetic and economic aspects of PVT-based building systems against PV and evacuated tube collectors. They revealed that the standalone PV system with the lowest levelized cost of energy of 89 €/MWh is the most economically superior option. Simulation and experimental assessment of PVT system and side-by-side conventional solar system (PV + collector) were investigated by Pokorny et al. [36] to find the best building-integrated model with the lowest dependency on the energy network. They found out that the roof-based PVT system is the preferable option in $CO_2$ emission reduction and higher renewable energy production. In another study, Kamel et al. [13] compared the performance criteria of PVT-driven smart buildings against PV-solar collector systems. They concluded that a remarkable increase in performance efficiencies and produced energy is achieved using the PVT system. However, a lower net present value is obtained compared to the side-by-side PV-collector.

In most of the applications of PV or PVT systems, a battery plus a heat pump are part of the energy system. Kamel and Fung [27] performed a comprehensive assessment of a zero-emission residential smart building equipped with PVT panels and an air source heat pump using the TRNSYS program. The results showed

that using the integration of PVT with heat pump leads to a decrease in 1734.7 kg $CO_2$ and 500 $ in annual greenhouse gas emission and electricity cost, respectively. However, the main problem of integrating PVT-driven building energy systems with heat pumps and batteries is their high cost. Herrando et al. [14] investigated the effect of economic variables on the cost competitiveness of building-integrated PVT systems equipped with battery and heat storage. They indicated that more than 35% of the system's total purchased cost corresponds to the PVT panels. A PVT-based combined cooling, heating, and power (CCHP) system integrated with a battery, heat pump, storage tank, and absorption chiller for three buildings were optimized and compared by Ren et al. [15], finding out that the battery and heat pump have a high contribution to the total investment cost. In another study, Arabkoohsar and Alsagri [16] proved that a heat pump could only be cost-efficient if it is used most of the time (a high utilization factor), which is not achievable for standalone systems.

Buildings with two-way interaction with the local energy grids are the main characteristic of smart energy systems, paving the path for truly having net-zero buildings, that is, buildings with (almost) zero emissions. A CCHP solar-based building system consisting of a PVT and a heat pump with two-way interaction with electricity, heat, and cooling networks was introduced and investigated by Zhang et al. [17]. They obtained a balance between the produced annual electricity, heat, and cooling productions and use with 109% supply of the total building's energy requirement. Lately, Gholamian et al. [18] proposed a near-zero smart CCHP building system equipped with the PVT interacting with energy grids. They showed that the proposed innovative configuration could supply the entire annual building's energy demand. Del Amo et al. [19] proposed a PVT-driven educational building in Italy having a two- and one-way interaction with electricity and heat networks, respectively. According to the results, about 60% of the building's total electricity and heat demand was provided by the solar system with a payback period of 15.4 years. Buonomano et al. [20] analyzed a dynamic building-integrated PVT system consisting of a heat pump, battery, and cooling absorption unit with two-way interaction with the electricity grid. They obtained a primary electricity and heating energy saving of 68.8% with 10.6 years payback period. Garcia et al. [21] introduced a zero-emission building located in central Europe comprising PVT panels, heat pumps, and storage tanks with two-way interaction with the district heating network. They revealed that the proposed configuration leads to a considerable increase in energy security and reduces the building's annual cost compared to the conventional heat pump system with no interaction with the heat network. Behzadi and Arabkoohsar [22] evaluated the feasibility of removing battery and heat pump from building-integrated PVT system interacting with electricity and district heating network simultaneously. They showed that the proposed innovative configuration could compensate for the building's annual electricity cost, and it has a considerable share in the local energy matrix due to the excess annual hot water of 402.8 $m^3$ sold to the district heating network.

Optimization of the system performance and sizing the components plays a crucial role, especially in thermal energy systems, because it increases performance efficiency and diminishes the system cost and environmental contamination [23,24]. The interaction between PVT panels/heat pump system combined with a heat storage tank was investigated by Dannemand et al. [25] to supply the domestic hot water and electricity need of a smart building in Denmark. They suggested that a parametric optimization and a better design of the storage tank result in a reduction in thermal losses in the system and more independence from the network. The simulation and experimental study of building-integrated PVT systems for Tunisian case were performed by Hazami et al. [26], finding out that 14.9% and 5.3% increase in hot water and electricity production is attained at the optimum operating condition. Techno-economic evaluation and multi-objective optimization of building-integrated PVT system combined with electricity storage were conducted by Chen et al. [27], contemplating energy and life cycle savings as objectives. They concluded that optimum sizing has a significant influence on system independence from the grid. A near zero-electricity/heat building-integrated PVT system combined with heat pump and thermal storage tank with two-way interaction with electricity grid was simulated by Sakellariou et al. [28]. They suggested optimizing the component's size should be more investigated to increase the cost-effective and share of solar energy in providing the building's demand. Behzadi et al. [29] optimized a building-integrated PVT system and indicated that the higher panel area and a lower storage tank volume lead to a better techno-economic condition. Also, they showed that at the optimum condition, the proposed system has a 4.03% higher exergy efficiency and 3.64 €/MWh lower total CHP cost.

Based on the literature review, it can be conceived that the main problem of solar-driven building energy systems is their insufficient cost-effectiveness, questioning their feasibility, and discouraging building proprietors economically. In order to address this, this study suggested a solar-based building energy system that stands on the following main pillars:

- Eliminating the battery of the system, which is a major source of expenditure of solar power systems.
- A creative method of heat pump integration, aiming at minimizing its required size and cost, with the highest possible utilization factor over the entire year.
- Using PVT-cooling (PVTC) panels tri-generating heat, electricity, and cooling based on natural heat transfer process toward the sky to cover the building’s entire energy demand and maximize the production rate per square meter.
- Having large-enough cold and heat storage units for higher self-sufficiency and minimizing the dependency on external support.

- Having a two-way interaction with electricity, heat, and cooling (if any) grids to practically compensate for the energy purchased from the energy distribution networks over an entire year.

Having the proposed concept of this article developed based on these principles, the sizing of its components and operation properties were optimized via multi-objective optimization methods. Further, the performance of the suggested system was techno-economic-environmentally investigated over an entire year. The performance of the optimized system was compared to the most competent solution in the same framework, using either PVT or PVTC panels integrated with heat and cold storage tanks, heat pump, and battery. To make the comparison fair, the optimization based on the genetic algorithm was applied to all the competing scenarios too. MATLAB was used for modeling and optimization in this study.

## 2. System description

Figure 1 demonstrates the schematic diagram of each building-integrated solar-driven system. The main components of each configuration were a PVT, a PVTC, a battery, an air-water heat pump, and heat and cold storage tanks. They differ based on the configuration, type of produced energy, presence or absence of electricity storage units or electricity-driven heat generator, and energy network they are interacting with. A detailed explanation of the studied configurations is given below:

a) Configuration 1 - with PVT, battery, and heat storage tank interacting with electricity and district heating network, as shown in Figure 1(a). In this configuration, the feasibility of integrating a PVT-driven system with a battery as the electricity storage unit, and a storage tank, as the heat storage unit is investigated. As depicted, based on examining the building's electricity/heat need and battery/heat storage tank capacity, the smart controller determines whether the electricity/heat should be stored in a battery/heat storage tank or provides the building's demand. Otherwise, when there isn't any electricity/heat and the battery/heat storage tank is full, the extra produced electricity/heat is sold to the electricity/district heating network.

b) Configuration 2 - with PVTC and heat and cold storage tanks interacting with electricity, heating, and cooling (if any) networks as presented in Figure 1(b). The solar PVTC panels are specific types of panels that tri-generate power, heat, and cold at a very high overall energy efficiency. In this configuration, the feasibility of eliminating the battery and heat pump on performance, economic, and environmental indicators is examined. Herein, the produced electricity first supplies the building's demand. Otherwise, it charges the electrical coil of the heat storage tank to produce hot water. The proposed configuration enjoys the heat and cold storage tanks to balance the heating and cooling energy between the panel, energy networks, and the building's demand.

c) Configuration 3 - with PVTC, air-water heat pump, and heat and cold storage tanks, as illustrated in Figure 1(c). In this configuration, the reversible air-water heat pump is applied to provide the

building's space heat and cooling demands when there isn't enough solar radiation or the storage tanks are vacant. The proposed configuration also interacts with the district heating network to supply the entire domestic hot water need or sell the extra heat produced by PVTC. Moreover, the produced electricity first provides the building's need and then runs the heat pump. In addition to the district heating network, this configuration interacts with the electricity grid in two-way to sell the extra electricity, provide the building's need, and drive the heat pump.

d) In Configuration 4, which has the same configuration as configuration 3, a new method of using heat pumps is introduced. In the proposed configuration, instead of a high-capacity heat pump for the entire building, a low-capacity one is used to simultaneously meet the building's demand interacting with the electricity grid.

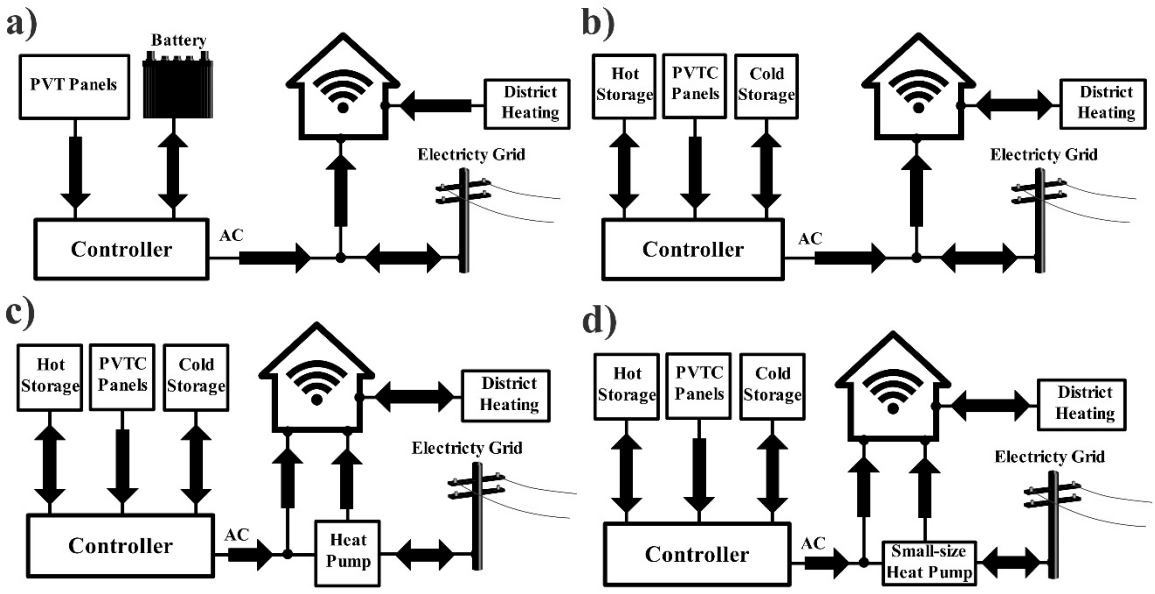


Figure 1. Schematic diagram of each configuration

## 3. Methodology

The thermodynamic, economic, and environmental assessment method for each configuration is presented in this section. . Finally, the tri-objective optimization applying the genetic algorithm was used to find the best operating condition of each configuration from techno-economic-environmental facets. The entire assessment approach was developed in MATLAB.

### 3.1. The case study

A 60-flat complex building located in Aarhus, Denmark, is contemplated as the case study investigating and comparing each solar-driven configuration's performance. The prerequisite data included the building's geometry, local weather information, thermal comfort, and the electricity demand profile to calculate the cooling and heat use profiles using TRNSYS software. The building geometry parameters, including the

number and height of flats on each floor and the flat, windows, walls, roofs, and floor areas, are listed in Table 1.

Table 1. The building geometry parameters.

| Parameter | Value |
|---|---|
| Flat numbers | 60 |
| Number of flats on each floor | 10 |
| Area of each flat ($m^2$) | 150 $m^2$ (10 m×15 m) |
| Height of each flat (m) | 3 |
| Windows area (%/shell) | 20 |
| Walls area (%/shell) | 30 |
| Roofs area (%/shell) | 25 |
| Floor area (%/shell) | 25 |

The hourly variation of the outdoor temperature, total solar irradiance, and the case study building hourly electricity use profile in Aarhus are presented in Figure 2. According to Figure 2(a), the outdoor temperature varies from -7.45ºC in the coldest hour till 29.08ºC in an hour in summer. What stands out from Figure 2 is that the solar irradiance increases up to 0.91 kWh/$m^2$ in the 4069$^{th}$ hour of the year. Figure 2(b) indicates that the maximum and minimum electricity load demands for the entire building are, respectively, 27.41 kWh and 8.69 kWh.

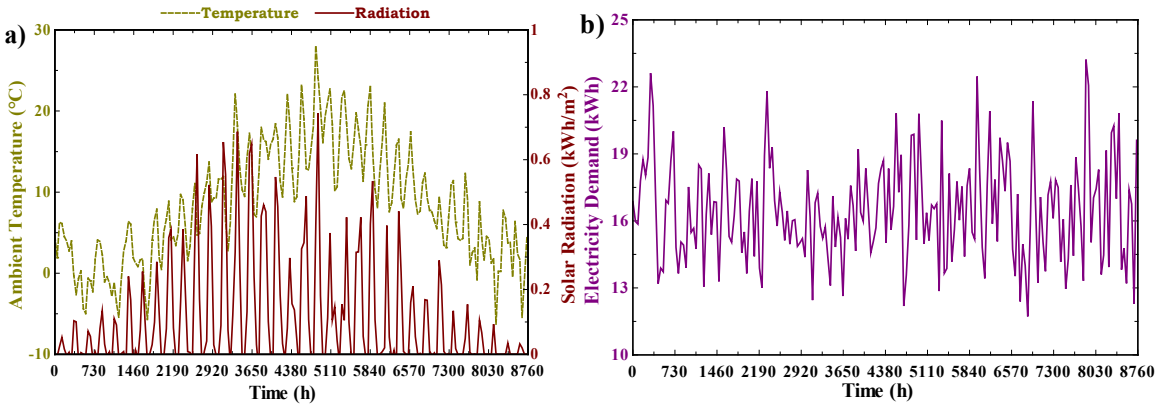


Figure 2. Hourly variation of a) outdoor temperature and total solar irradiance b) electricity demand of the entire building located in Aarhus

### 3.2. Modeling approach

Thermodynamic assessment is carried out by developing the mass and energy balances for each component as a control volume as follow [30]:

$$\sum \dot{m}_{in} = \sum \dot{m}_{out} \quad (1)$$

$$\dot{Q} - \dot{W} = \sum \dot{m}_{out}\, h_{out} - \sum \dot{m}_{in}\, h_{in} \quad (2)$$

where $\dot{m}$ is the mass flow rate, and $\dot{Q}$ and $\dot{W}$ is the heat transfer rate to/from and the work done by/on the control volume.

### *3.2.1. Building model*

The energy balance for a zone, which is the basis of the building's heating and cooling loads calculation, can be calculated by the following equation [31]:

$$m_{air} C_{p,air} \frac{dT_z}{dt} = \dot{Q}_{equipments} + \dot{Q}_{surfaces} + \dot{Q}_{zones} + \dot{Q}_{amb} + \dot{Q}_{system} \quad (3)$$

In this equation, $T_z$, $m_{air}$, $C_{P,air}$, and $\dot{Q}_{sys}$ are the zone temperature, air mass flow rate, the specific heat of air, and heating/cooling energy provided by the source. Moreover, $\dot{Q}_{equipments}$, $\dot{Q}_{surfaces}$, $\dot{Q}_{zones}$, and $\dot{Q}_{amb}$ are the internal convective gains (by equipment and people), surface convective heat transfer, heat transfer of mixing air came from other zones, infiltration gains (airflow from outside only), and can be calculated as following, respectively:

$$\dot{Q}_{equipments} = \sum_{i=1}^{N_{equipment}} \dot{m}_i C_p \left(T_{equipment,i} - T_z\right) \quad (4)$$

$$\dot{Q}_{surfaces} = \sum_{i=1}^{N_{surfaces}} h_i A_i (T_{surface,i} - T_z) \quad (5)$$

$$\dot{Q}_{zones} = \sum_{i=1}^{N_{zones}} \dot{m}_i C_p \left(T_{z,i} - T_z\right) \quad (6)$$

$$\dot{Q}_{amb} = \dot{m}_{amb} C_p (T_{amb} - T_z) \quad (7)$$

Detailed information about the thermodynamic equations for evaluating the building's heating and cooling demands can be found in the TRNSYS documents [31].

### *3.2.2. Solar panel model*

The PVT panel's mathematical model as the primary mover of each configuration is investigated in detail. According to Figure 3, the absorbed solar radiation is divided into four parts: the heat lost to the ambient through the convection ($\dot{Q}_{loss,top,conv}$), the heat lost to the sky via radiation ($\dot{Q}_{loss,top,rad}$), the heat lost to the back plate by conduction ($\dot{Q}_{loss,back,cond}$), and the useful energy gain by the coolant fluid entering the panel ($\dot{Q}_{useful}$).

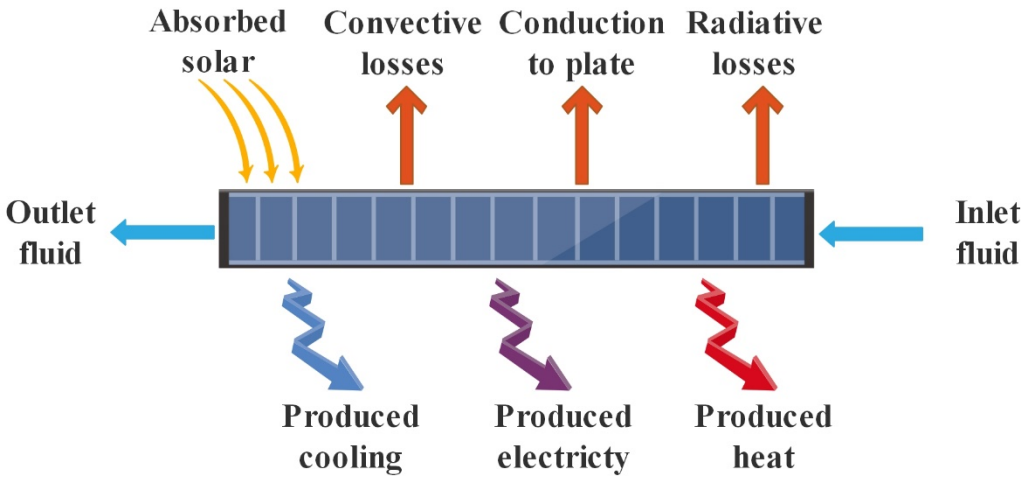


Figure 3. Energy flows on the PVTC/PVT surface.

Therefore, the energy balance on the PVT panel surface is written as below [32]:

$$\dot{Q}_{absorbed} = \dot{Q}_{loss} + \dot{Q}_{useful} \quad (8)$$

$$\dot{Q}_{loss} = \dot{Q}_{loss,top,conv} + \dot{Q}_{loss,top,rad} + \dot{Q}_{loss,back,cond} \quad (9)$$

Here $\dot{Q}_{absorbed}$ is the net absorbed solar radiation, which is equal to the absorbed solar radiation minus the PV power production as following [33]:

$$Q_{absorbed} = GA(\tau\alpha)(1 - \eta_{PV}) \quad (10)$$

Here $G$ is the total radiation on a tilted surface, $A$ is the panel area, and $\tau\alpha$ denotes the transmittance-absorptance coefficient. In addition, $\eta_{PV}$ is the PV panel cell efficiency depending on nominal condition, cell temperature, and solar radiation as follow [31]:

$$\eta_{PV} = \eta_{nominal} X_T X_R \quad (11)$$

$$X_T = 1 + Eff_T(T_{PV} - T_{ref}) \quad (12)$$

$$X_R = 1 + Eff_G(G_T - G_{ref}) \quad (13)$$

Furthermore, the produced power by the panel is calculated as below [31]:

$$W_{PVT} = GA(\tau\alpha)\eta_{PV} \quad (14)$$

Eventually, the remaining heat transfers for the panel are written as [31]:

$$Q_{loss,top,conv} = h_{outer} A(\bar{T}_{PVT} - T_{amb}) \quad (15)$$

$$Q_{loss,top,rad} = h_{rad} A(\bar{T}_{PVT} - T_{sky}) \quad (16)$$

$$Q_{loss,back} = A\frac{\bar{T}_{abs} - \bar{T}_{inside}}{R_B} \quad (17)$$

$$Q_u = \dot{m}\, C_P(T_{fluid,out} - T_{fluid,in}) \quad (18)$$

Where $R_B$ is the resistance to heat transfer from the absorber via the back of the panel and $h_{outer}$ is the convective heat transfer coefficient from the top of the panel to the ambient temperature. $h_{rad}$, which is the radiative heat transfer coefficient from the top of the panel to the sky, is calculated as follows [34]:

$$h_{rad} = \varepsilon\sigma(T_{PVT} + T_{sky})(T_{PVT}^2 + T_{sky}^2) \quad (19)$$

In which $\varepsilon$ and $\sigma$ are, respectively, the emissivity at the top of the panel and Stefan-Boltzmann constant.

In addition to power and heat production in the day, the PVTC panel can produce cooling energy via the cold sky's radiation at night (look at Figure 3). This is reasonable because the panel temperature falls beneath the sky temperature at night and the heat transfer takes place in the reverse direction of the day. The cooling power is calculated as follows [35]:

$$\dot{Q}_{PVTC} = \dot{Q}_{rad} + \dot{Q}_{conv} \quad (20)$$

here $\dot{Q}_{rad}$ is the radiative heat transfer and $\dot{Q}_{conv}$ is the convective heat transfers, which is calculated as:

$$\dot{Q}_{conv} = A\, h_{c,mix}(T_{PVTC} - T_{amb}) \quad (21)$$

In which, $h_{c,mix}$ is the convective heat transfer coefficient and is calculated as below [36,37]:

$$h_{c,mix} = \sqrt[3]{h_{c,forced}^3 + h_{c,nat}^3} \quad (22)$$

$$h_{c,forced} = 2.8 + 3\, U_w \quad (23)$$

$$h_{c,nat} = 1.78\, (T_{PVTC} - T_{amb})^{1/3} \quad (24)$$

Where $h_{c,forced}$ and $h_{c,nat}$ are natural and forced convective heat transfer coefficients, and $U_w$ is the wind velocity.

### *3.2.3. Heat pump model*

To model the heat pump, the coefficient of performance (COP) was used based on the Lorenz equation as follows:

$$COP = \eta_{Lorenz} \times COP_{Lorenz} \quad (25)$$

For heat production: $COP_{Lorenz} = \frac{T_{lm,H}}{T_{lm,H} - T_{lm,c}}$ (26)

For cold production: $COP_{Lorenz} = \frac{T_{lm,C}}{T_{lm,H} - T_{lm,c}}$ (27)

Here $\eta_{Lorenz}$ is the Lorenz efficiency as the ratio between the actual and Lorenz coefficients of performance, and $T_{lm}$ is the logarithmic (entropic) mean temperature which can be evaluated as:

$$T_{lm,C} = \frac{T_{C,out} - T_{C,in}}{\ln T_{C,out} - \ln T_{C,in}} \quad (28)$$

$$T_{lm,H} = \frac{T_{H,out} - T_{H,in}}{\ln T_{H,out} - \ln T_{H,in}} \quad (29)$$

*3.2.4. Total cost calculation*

After developing the mathematical equation of each component, the performance assessment and comparison of each configuration was carried out by evaluating the total sold and purchased energy to and from networks and primary energy saving rate as below [15]:

$$Net\ bought\ energy = \dot{E}_{Purchased} + \dot{Q}_{Purchased} \quad (30)$$

$$Net\ sold\ energy = \dot{E}_{Sold} + \dot{Q}_{Sold} \quad (31)$$

$$PESR = \frac{F^{SP} - F^{Solar}}{F^{SP}} \times 100 \quad (32)$$

Here $F^{SP}$ is the fuel used for electricity and heat demands supplied from electricity and district heating networks, and $F^{Solar}$ is the solar energy of each proposed solar-driven building system, which are calculated as:

$$F^{SP} = \frac{\dot{E}_{Demand}}{\eta_E \eta_{grid}} + \frac{\dot{Q}_{Demand}}{\eta_H \eta_{grid}} \quad (33)$$

$$F^{Solar} = \frac{\dot{E}_{Purchased}}{\eta_E \eta_{grid}} + \frac{\dot{Q}_{Purchased}}{\eta_H \eta_{grid}} - \dot{E}_{Sold} - \dot{Q}_{Sold} \quad (34)$$

In which, $\eta_E$ and $\eta_H$ are the electrical and heat efficiencies of the CHP waste to the energy plant as the conventional way in Denmark and $\eta_{grid}$ is the network's energy transmission efficiency.

## 3.3. Economic analysis

The specific cost theory was implemented to conduct the economic evaluation. According to the theory, the cost of each component ($Z_k$) equals the sum of capital investment ($Z_k^{CI}$) and operating and maintenance costs ($Z_k^{OM}$) as below [38]:

$$Z_k = Z_k^{CI} + Z_k^{OM} \quad (35)$$

$$Z_k^{OM} = \gamma_k Z_k \quad (36)$$

Here $\gamma$ is the fixed costs coefficient. Table 2 presents the capital investment cost of each component to accomplish the economic evaluation.

Table 2. Purchased cost of each component of each configuration [39–41].

| **Component** | $Z_k$ **($)** |
|---|---|
| Battery lithium-ion | 8800 |
| Air-Water Heat Pump | $Z_{HP}=c_1 \times CAP_{HP}$<br>$c_1$=560 $/kWh |
| PVT Panel | $Z_{PVT}=c_2 \times A_{PVT}$<br>$c_2$=448 $/m$^2$ |
| Cold Storage | $Z_{CSt}=c_3 \times CAP_{CSt}$<br>$c_3$=105.6 $/kWh |

| | |
|---|---|
| Heat Storage | $Z_{HSt}=c_4\times CAP_{HSt}$<br>$c_4$=105.6 \$/kWh |

After determining each component's cost, the economic comparison of each configuration is examined based on the assessment of the annual cost saving rate, net present value, and payback period. To begin with, the annual cost saving rate as the yearly benefit of each solar-based hybrid building system compared with separation production system is calculated as following [15]:

$$ACSR = \frac{AC^{SP} - AC^{Solar}}{AC^{SP}} \times 100 \quad (37)$$

In which $AC^{SP}$ and $AC^{Solar}$ are the annual cost of separation production and solar-based systems, respectively, which are written as:

$$AC^{SP} = \dot{E}_{Demand} \times c_{electricty} + \dot{Q}_{Demand} \times c_{heat} \quad (38)$$

$$AC^{Solar} = \left(\dot{E}_{Bought} - \dot{E}_{Sold}\right) \times c_{electricty} + \left(\dot{Q}_{Bought} - \dot{Q}_{Sold}\right) \times c_{heat} \quad (39)$$

Here $c_{electrcity}$ and $c_{heat}$ are the electricity and heat prices which are, respectively, 400 \$/MWh and 69.6 \$/MWh in Denmark. Moreover, the net present value over 40 years to assess the cost-effectiveness of each configuration is calculated as below:

$$NPV = \sum_{i=1}^{40} \frac{AC_i^{Reduced} - \dot{Z}_{tot,i}^{OM}}{(1+r)^i} - \dot{Z}_{tot}^{CI} \quad (40)$$

Where $r$ is the discount rate, and $AC_{Reduced}$ is the reduced annual cost as the difference between the annual cost of separation production and solar-based systems as follow:

$$AC^{Reduced} = AC^{SP} - AC^{Solar} \quad (41)$$

Last but not least economic indicator is the payback period ($PP$), which is equal to the number of years needed to reimburse the initial costs and written as:

$$PP = \frac{C_{tot}}{AC^{Reduced}} \quad (42)$$

$$C_{tot} = \sum_{k=1}^{n_k} Z_k \quad (43)$$

Here, $C_{tot}$ is the total cost equal to the sum of each component's cost.

### 3.4. Environmental analysis

Due to the worrying increment in worldwide environmental pollution and the hazardous impact of global temperature increment resulting from greenhouse gas emissions, environmental analysis has become more significant than ever. Herein, the carbon dioxide emission reduction rate is calculated based on Eq. (39) to

compare the proposed building-integrated solar-driven configurations and indicate their superiority against the conventional systems.

$$CDERR = \frac{CDE^{SP} - CDE^{Solar}}{CDE^{SP}} \times 100 \quad (44)$$

In which $CDE^{SP}$ and $CDE^{Solar}$ are the carbon dioxide emission of separation production and solar-based systems in kg which are evaluated as, respectively:

$$CDE^{SP} = \dot{E}_{Demand} \times \lambda_{electricty} + \dot{Q}_{Demand} \times \lambda_{heat} \quad (45)$$

$$CDE^{Solar} = \left(\dot{E}_{Bought} - \dot{E}_{Sold}\right) \times \lambda_{electricty} + \left(\dot{Q}_{Bought} - \dot{Q}_{Sold}\right) \times \lambda_{heat} \quad (46)$$

$\lambda_{electricty}$ and $\lambda_{heat}$ are the $CO_2$ emission coefficients equal to 166 kg/MWh and 105.6 kg/MWh, respectively, for Denmark [29].

### 3.5. Multi-objective optimization

A multi-objective optimization method is a potent tool dealing with mathematical optimization problems, including more than one objective to be optimized at the same time. It has been implemented in many engineering fields, like thermal energy systems, where optimal decision variables should be determined in the existence of trade-offs between conflictive objectives. Indeed, decision-makers try to minimize the system cost while maximizing the performance efficiencies or minimizing the cost and environmental indicators simultaneously in thermal engineering systems. Of all kinds of optimization approaches, the genetic algorithm is the most robust option because of the highest computation speed and minimum fitness for the same problem. It also has the best performance in solving problems that other methods are unable to solve.

In the present study, tri-objective optimization using a genetic algorithm approach is implemented in each configuration to determine the best operating condition from techno-economic-environmental viewpoints simultaneously. MATLAB software is applied to each configuration to minimize the total cost rate (Eq. (43)) and total purchased energy from the networks (Eq. (30)) while maximizing the carbon dioxide emission reduction rate (Eq. (44)) simultaneously.

## 4. Results and discussions

The performance, economic, and environmental assessment of each configuration is surveyed using MATLAB software. Annual and monthly values of techno-economic-environmental indicators are calculated for a 60-flat complex building in Aarhus to find the best configuration from various viewpoints. A parametric study was also accomplished to investigate and compare each configuration's variation of

performance indicators with significant decision parameters. Eventually, the tri-objective optimization based on the genetic algorithm approach was applied to each configuration to obtain the optimum condition contemplating performance, economic, and environmental aspects as objectives simultaneously. The relevant assumptions and operating parameters of every component of each system are tabulated in Table 3.

Table 3. The operating parameters of each subsystem.

| Parameter | Value |
|---|---|
| Panel area ($m^2$) | 18 |
| Number of panels for the whole building | 50 |
| Lithium-ion battery capacity (kWh) | 300 |
| Battery volume ($m^3$) | 0.77 |
| Heat storage capacity (kWh) | 400 |
| Heat storage volume ($m^3$) | 5.76 |
| Cold storage capacity (kWh) | 400 |
| Cold storage volume ($m^3$) | 5.76 |
| Heat pump capacity (kWh) | 40 |

4.1. Time-dependent results

The hourly values of heat and cooling demands for the proposed case study complex building over the entire year calculated by TRNSYS software are illustrated in Figure 4. According to the figure, because the heating demand is a function of the outdoor temperature, it decreased from Winter to Summer and increases in Autumn. Figure 4 indicates that the heat demand varies from the baseload value of 10.04 kW to 196.5 kW. In contrast, since the outdoor temperature increased in Spring and Summer, the cooling load demand increased. As presented in Figure 4, the cooling load demand reaches up to the maximum value of 101.6 kW in the $4547^{th}$ hour of the year.

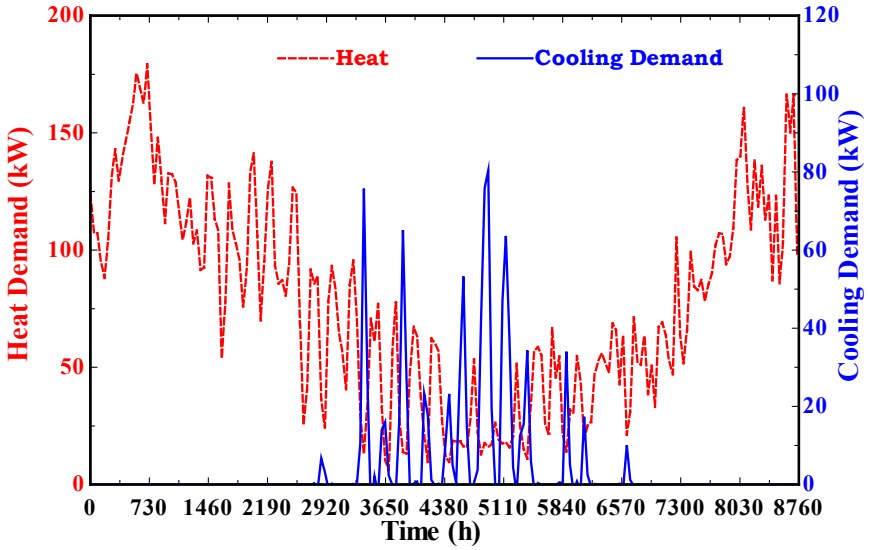


Figure 4. Hourly variation of heat and cooling demand calculated for the 60-flat complex building over the year

The yearly side-by-side comparison of the total sold/purchased energy to/from networks, total cost, primary energy saving ratio, annual cost-saving ratio, carbon dioxide emission reduction ratio, and payback period for each configuration is depicted in Figure 5. According to Figure 5(a), configuration 1 and configuration 2 have the highest total cost of 784,944 $ and 626,834.2 $, respectively, due to the use of battery and heat pump, two significant sources of investment costs. The figure further indicates that configuration 4 has a higher total cost of 25,875 $ compared to configuration 2 because of the presence of a cold storage unit. Figure 5(b) reveals that configuration 1 has the lowest total sold energy to the networks of 87.3 MWh, indicating the excellence of using PVTC against PVT panels from the performance facet due to the simultaneous production of heat, electricity, and cooling energy simultaneously. The figure further shows that the lowest purchased total energy corresponds to configuration 3, which is integrated with the heat pump providing the heat demand due to the lowest purchased heat from the district heating network. A higher sold energy and lower purchased energy result in a higher primary energy saving, as inferred from Eq. (22). Therefore, configuration 3 and configuration 4, comprising PVTC and heat pump with the highest PESR of 86.9% and 71.1%, respectively, are the best models from the performance facet, as depicted in Figure 5(c). The figure also demonstrates that configuration 1, with the lowest PESR of 46.3%, is the worst from a performance standpoint.

Furthermore, the figure shows that configuration 3 and configuration 4 are the most environmental-friendly systems due to the highest carbon dioxide emission reduction rate of 117.7% and 103.5%. Finally, it can be obtained that configuration 2 and configuration 4, which are not equipped with battery and heat pumps, are the most economical option because of the lowest payback period of 6.2 years and 6.3 years. This

indicates the excellence of the battery and heat pump removal in motivating the building owners to invest in such systems.

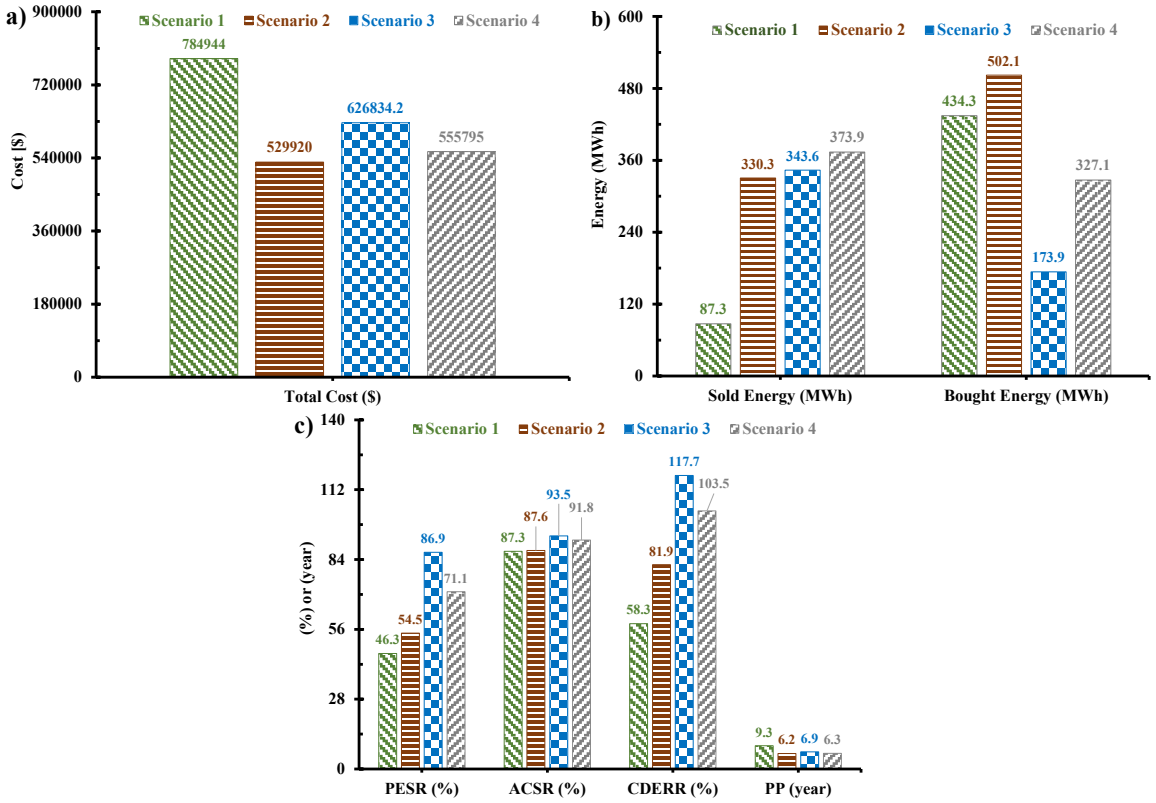


Figure 5. The comparison of a) total cost, b) sold/purchased energy to/from networks, and c) primary energy saving ratio, annual cost-saving ratio, carbon dioxide emission reduction ratio, and payback period for each configuration

Figure 6 illustrates the monthly comparison of total purchased/sold energy from/to networks for each configuration. More solar radiation leads to more useful energy absorbed by the panel; therefore, for each configuration, the value of sold energy to networks increases from January to June up to a specific value and then decreases from June to December, as shown in the graph. Conversely, by decreasing the solar availability and ambient temperature from summer to winter, the system dependence on energy networks increases to supply the building's demand; hence, the value of purchased energy from the networks increases for each configuration, as demonstrated in Figure 6. The figure further shows that configuration 3, which is equipped with a heat pump, needs the minimum energy from the networks among all models. Moreover, while configuration 4, which is integrated with a new method of using a heat pump, has the highest sold energy to networks, configuration 1, driven by PVT panels, has the lowest sold energy to the networks in the whole year. According to the figure, while configuration 4 has the maximum sold energy

of 88.7MWh in June, the maximum monthly purchased energy of 89.9 MWh corresponds to configuration 1 in January.

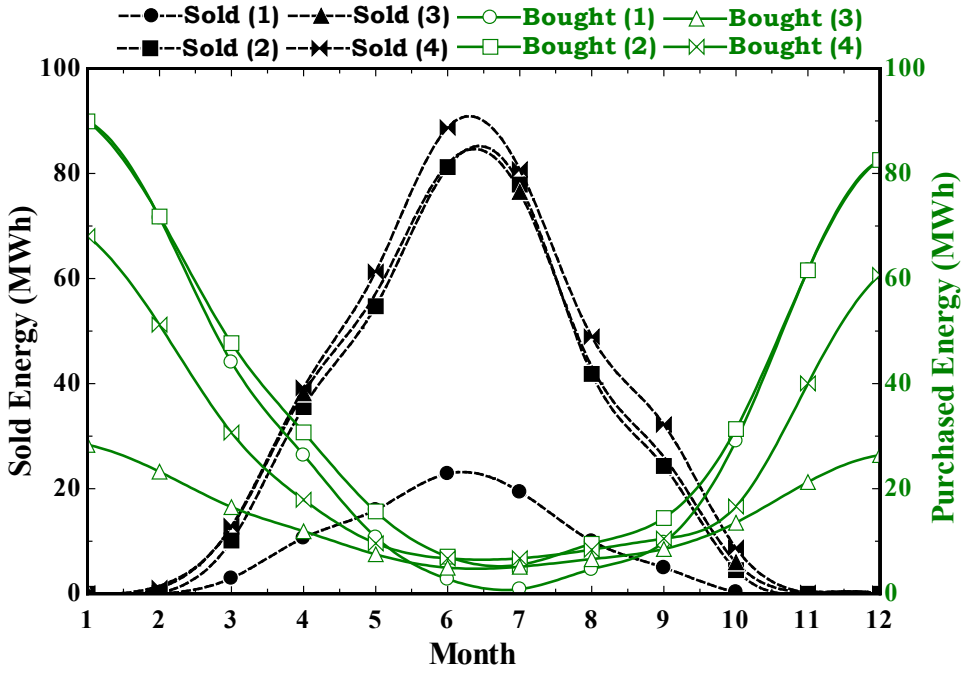


Figure 6. Monthly variation of sold and purchased total energy to and from networks for each configuration

A significant indicator to assess and compare the cost-effectiveness of each configuration is the net present value. The comparison of NPV for each configuration over 40 years is indicated in Figure 7. According to the graph, configuration 4 and configuration 2 are the best models from an economic standpoint because in the shortest time (9.4 years), their NPV goes from negative to zero. Also, the NPV of configuration 3 and configuration 1 will be zero after 10.8 years and 18.6 years, respectively, indicating that the use of the battery and heat pump is not economically favorable.

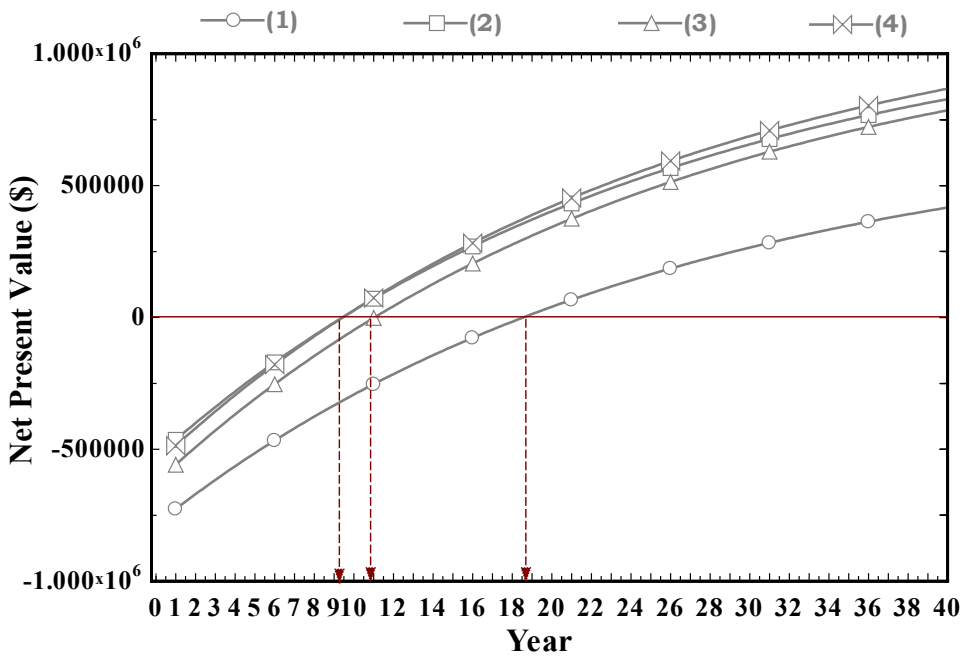

Figure 7. Variation of net present value for each configuration over 40 years.

4.2. Parametric study of the system configurations

The effect significant decision parameters containing panel area, heat storage, and cold storage tanks capacity, and battery capacity on the performance of each configuration is studied and compared by evaluating their impact on purchased energy, primary energy saving ratio, total cost, annual cost-saving ratio, payback period, and carbon dioxide emission reduction ratio as techno-economic-environmental objectives.

Because the panel's physical characteristic plays a vital role in solar energy conversion, the influence of the panel area on the performance of each configuration is investigated and compared in Figure 8. According to Eq. (5), when the panel area increases, the net absorbed solar radiation and the value of net produced energy (electricity+heat) increase too. Therefore, the system dependence on solar-driven technologies increases, and the value of purchased energy from the networks decreases, as demonstrated in Figure 8(a). The figure also indicates that as the panel area increases, PESR increases for each configuration. This is rational because by increasing the area, the net sold energy increases, and the model's performance will improve. According to Figure 8(b), the increase in panel area leads to an increase in total cost, which is not economically favorable. This is reasonable because the panel's purchased cost increases as the area increase. The figure also indicates that a higher panel area for each configuration leads to an increase in ACSR and CDERR because of a lower value of purchased energy from networks. It is noted that by increasing the panel area, the simultaneous increase in CDERR, which is favorable, and total cost,

which is not desirable, illustrates the significance of the multi-objective optimization method trying to find a trade-off between conflictive objectives.

Furthermore, Figure 8(c) shows that when the panel area increases, each configuration's initial investment cost is reimbursed in fewer years, so the payback period decreases. The figure also indicates that in the selected range of panel area, due to the lower total cost and payback period of configuration 2 and configuration 3 compared to the corresponding values of configuration 1 and configuration 3, a favorable economic condition is achieved by eliminating battery and heat pump. It can be further concluded that configuration 4, driven by PVTC with a new method of using a heat pump, is the best configuration from performance, economic, and environmental points of view.

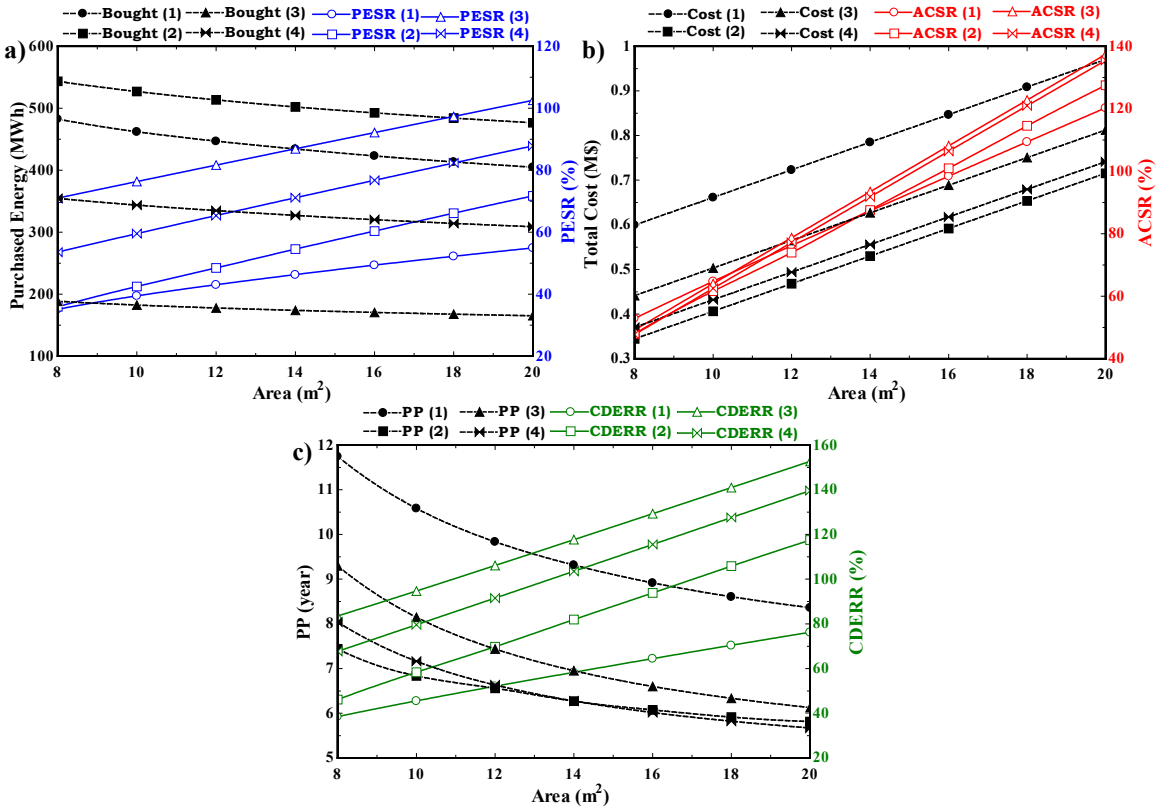


Figure 8. The variation of a) purchased energy and primary energy saving ratio b) total cost and annual cost-saving ratio c) payback period and carbon dioxide emission reduction ratio for each configuration with the area of the panel

In Figure 9, the variation of purchased energy, primary energy saving ratio, total cost, annual cost-saving ratio, payback period, and carbon dioxide emission reduction ratio with heat storage capacity is shown. According to Figure 9(a), by increasing the heat storage capacity from 200 kWh to 600 kWh, the district heating network's net purchased heat decreases. Thus, a lower net purchased total energy, and a higher PESR are achieved. Figure 9(b) demonstrates that as the heat storage capacity increases, the total cost increases for each configuration. This is justified because the use of a bigger heat storage tank leads to a

higher investment cost. The figure also depicts that while picking up the heat storage capacity results in a higher ACSR, the CDERR for each configuration is reduced. Figure 9(c) shows that when the heat storage capacity increases from 200 kWh to 600 kWh, the payback period's value increases for each configuration that is not economically suitable. Like the previous figure, configuration 4 and configuration 2 are the best models from the economic facet due to the lowest total cost and payback period in the whole range of heat storage capacity. It can also be obtained that configuration 3 is the best option from the performance aspect standalone due to the lowest purchased energy from the networks and PESR.

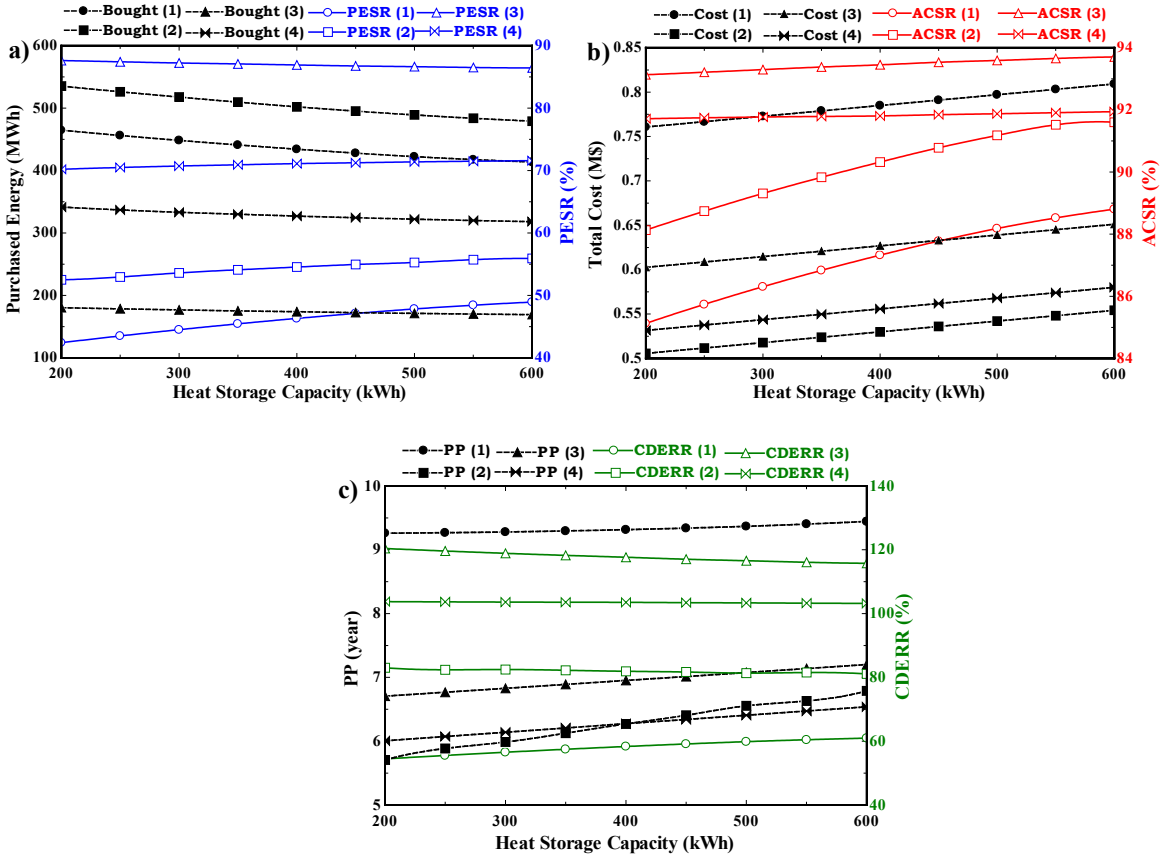


Figure 9. The variation of a) purchased energy and primary energy saving ratio b) total cost and annual cost-saving ratio c) payback period and carbon dioxide emission reduction ratio for each configuration with the heat storage capacity

Figure 10 depicts the variation of performance/economic/environmental indicators of configuration 1 with the battery capacity. The more battery capacity leads to a more possibility of storing electricity, so the net purchased energy from the networks decreases, and better performance is obtained, as demonstrated in Figure 10(a). The figure shows that by increasing the battery capacity from 100 kWh to 500 kWh, the purchased energy decreases from 452.5 MWh to 432 MWh, and the PESR increases from 43.6% to 46.8%. In contrast, since the purchased cost of battery increases with an increase in battery capacity, the total cost

and the payback period of configuration 1 will increase from 0.58 M$ to 0.98 M$ and 7 years to 11.5 years, respectively, as shown in Figure 10(b) and Figure 10(c). Furthermore, it can be concluded that the increase of battery capacity from 100 kWh to 500 kWh has a positive effect on the model's environmental aspect due to the increase of CDERR from 57.6% to 58.9%. Moreover, the conflictive variation between the objectives, i.e., an increase in total cost while decreasing purchased energy, discloses the importance of multi-objective optimization.

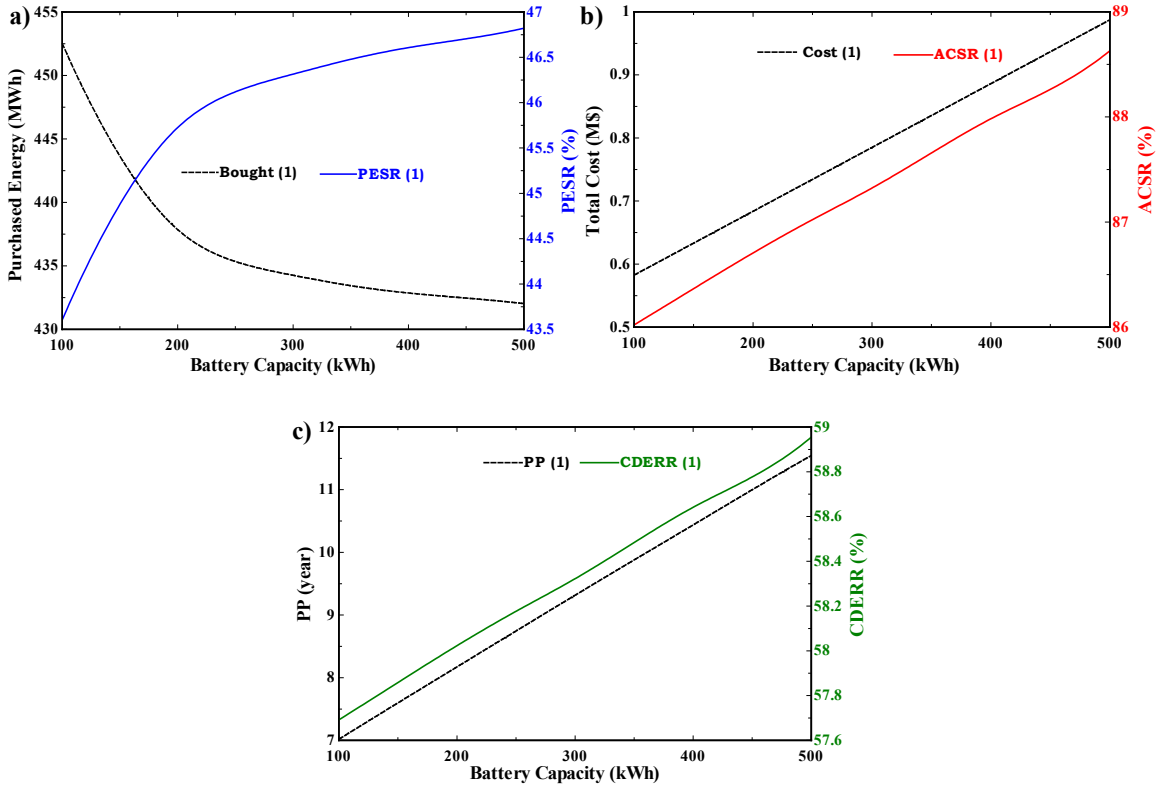


Figure 10. The variation of a) purchased energy and primary energy saving ratio b) total cost and annual cost-saving ratio c) payback period and carbon dioxide emission reduction ratio for configuration 1 with the battery capacity

The influence of cold storage capacity on configuration 2, configuration 3, and configuration 4, equipped with PVTC panels producing electricity, heat, and cooling, is presented in Figure 11. According to the figure, the variation of cold storage capacity from 200 kWh to 600 kWh does not alter the purchased energy from the networks, PESR, and CDERR considerably for each configuration. The more cold storage capacity results in a higher investment cost, so the total cost and payback period increase about 0.05 M$ and 5 years for each configuration as depicted in the figure. Furthermore, Figure 11(b) indicates that by increasing the capacity, the ACSR of configuration 3 and configuration 4 increase less than 0.4%, which is not considerable. Finally, same as the previous figures, it can be concluded that configuration 4 and

configuration 2 are economically superior compared to configuration 3 due to the lower payback period and total cost in the whole domain of cold storage capacity.

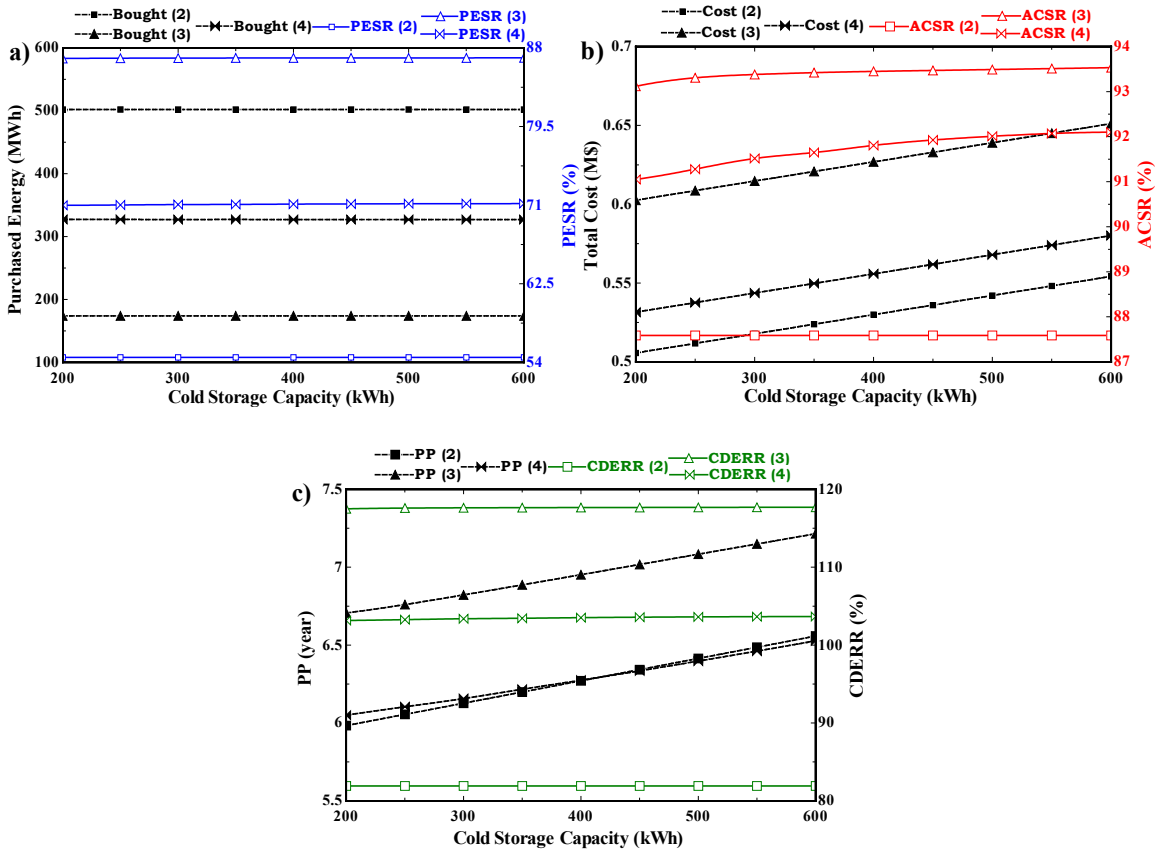


Figure 11. The variation of a) purchased energy and primary energy saving ratio b) total cost and annual cost-saving ratio c) payback period and carbon dioxide emission reduction ratio for configuration 1 with the cold storage capacity

### 4.3. Optimization results

The tri-objective optimization based on a genetic algorithm was implemented to each configuration, considering total purchased energy from the network to be minimized, carbon dioxide emission reduction rate to be maximized, and the total cost to be minimized as objectives. The logical domain of significant decision parameters, including panel area, battery capacity, heat, and cold storage tank capacities, are tabulated in Table 4.

Table 4. The domain of significant decision parameters of each configuration

| Parameter | Lower bound | Higher bound |
|---|---|---|
| Panel area ($m^2$) | 8 | 20 |
| Battery capacity (kWh) | 100 | 500 |
| Heat storage capacity (kWh) | 200 | 600 |
| Cold storage capacity (kWh) | 200 | 600 |

Figure 12 demonstrates the Pareto frontier diagram of net purchased energy, CDERR, and total cost for each configuration. According to the figure, the ideal point is defined as the conjunction of minimum total purchased energy from the networks, maximum CDERR, and minimum total cost. Because the ideal point is not on the Pareto curve, of all optimum points, the nearest one with the lowest normalized distance is chosen as the most favorable solution (best point).

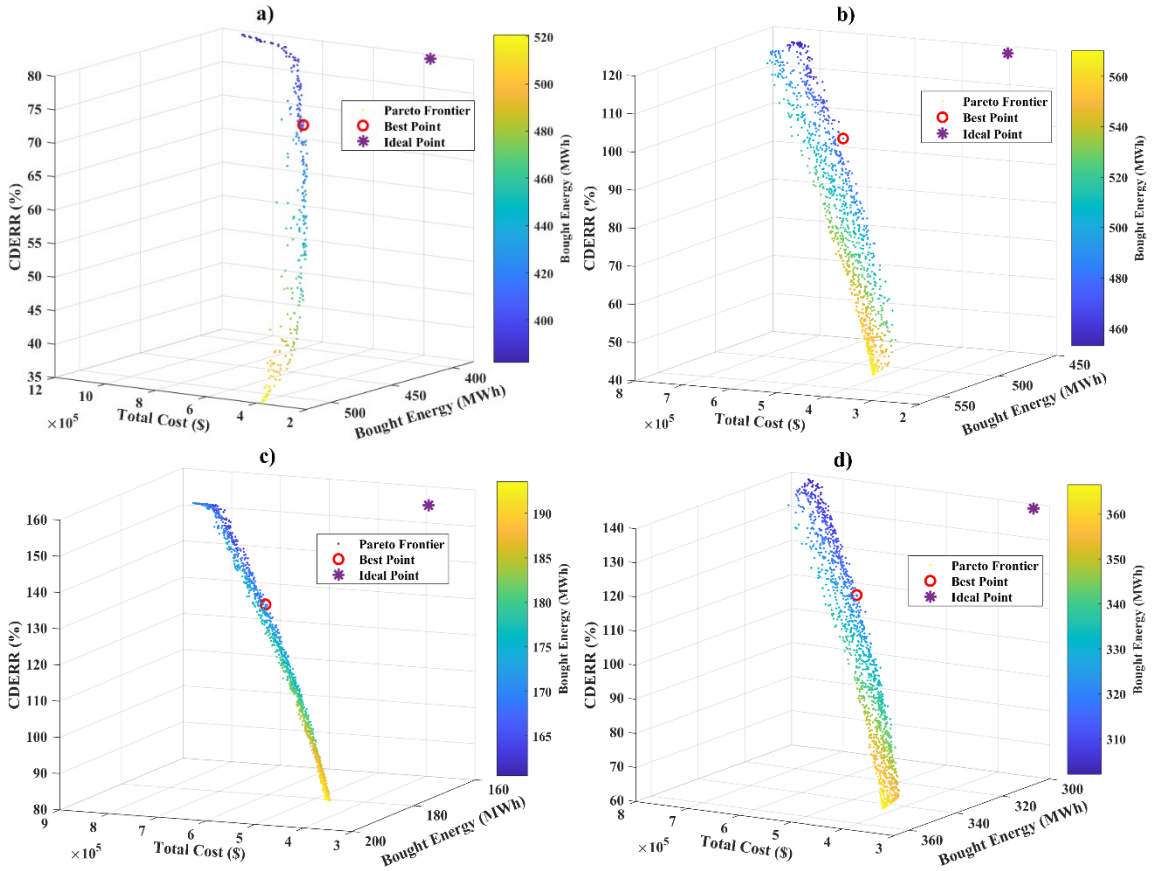


Figure 12. Pareto frontier diagram of carbon dioxide emission reduction rate, purchased energy, and total cost for a) configuration 1, b) configuration 2, c) configuration 3, and d) configuration 4

The two-dimensional Pareto projection of carbon dioxide emission reduction rate purchased energy and the total cost is illustrated in Figure 13 to better comprehend the Pareto frontier diagram.

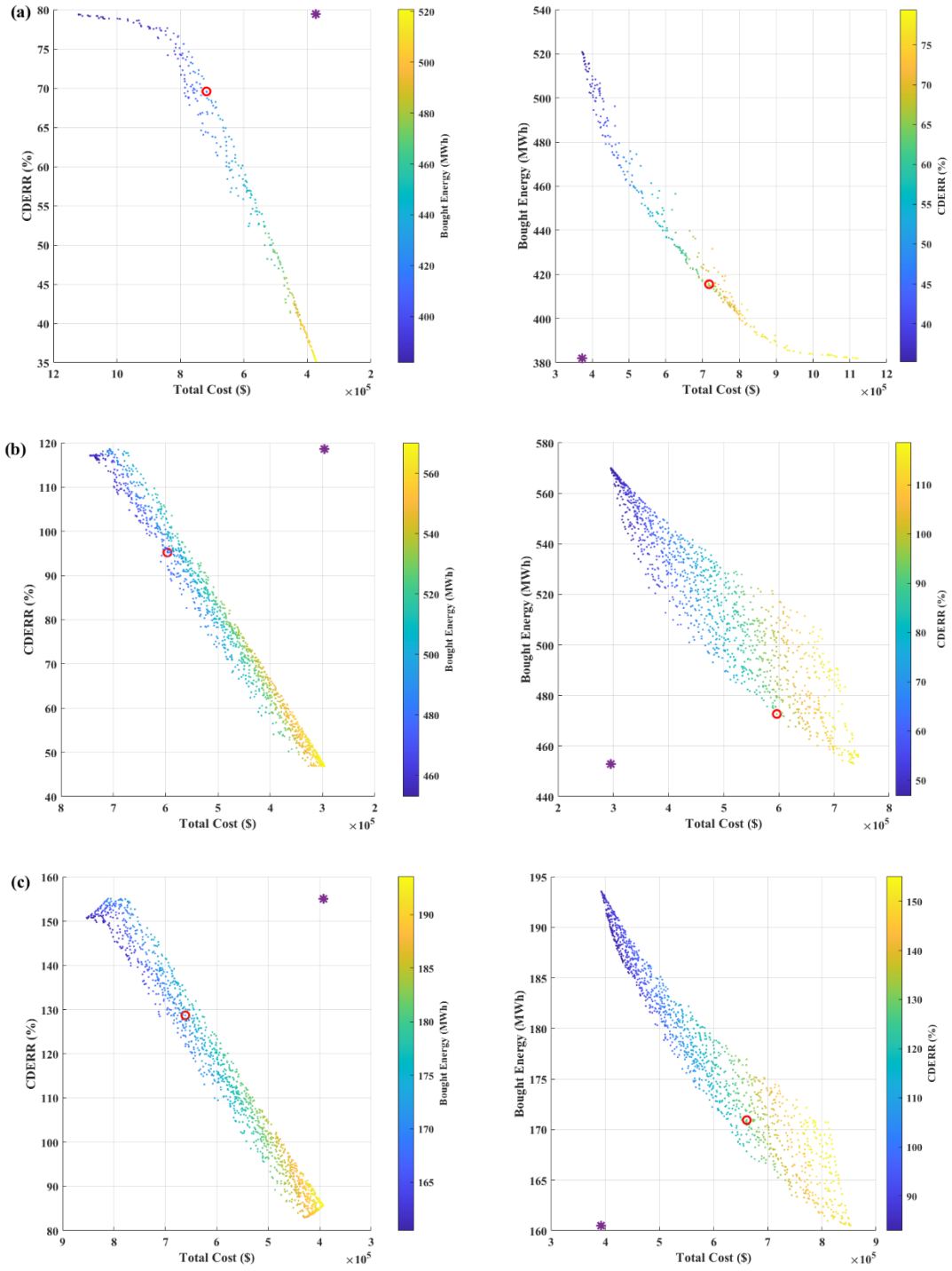
(a)
CDERR (%)
Total Cost ($)
×10^5
Bought Energy (MWh)
Bought Energy (MWh)
Total Cost ($)
×10^5
CDERR (%)
(b)
CDERR (%)
Total Cost ($)
×10^5
Bought Energy (MWh)
Bought Energy (MWh)
Total Cost ($)
×10^5
CDERR (%)
(c)
CDERR (%)
Total Cost ($)
×10^5
Bought Energy (MWh)
Bought Energy (MWh)
Total Cost ($)
×10^5
CDERR (%)

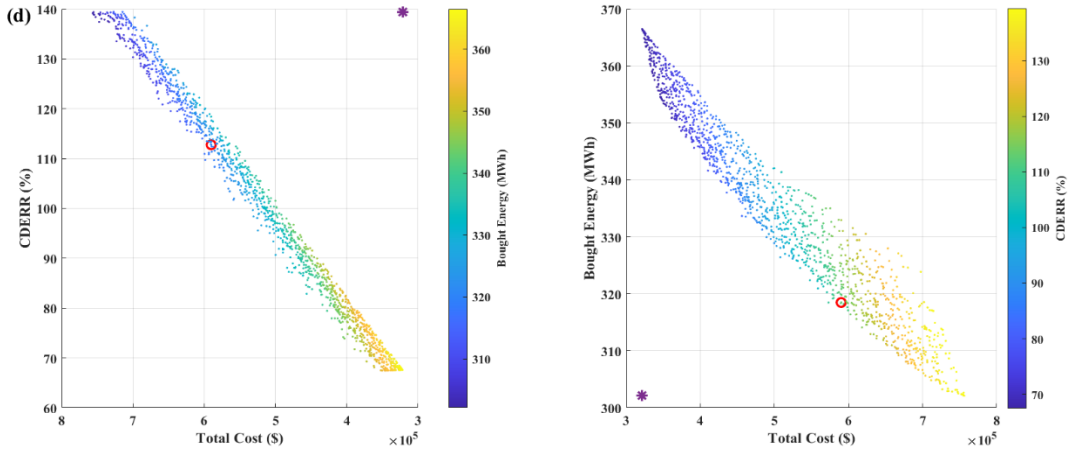


Figure 13. Two dimensional Pareto projection of carbon dioxide emission reduction rate, purchased energy, and total cost for a) configuration 1, b) configuration 2, c) configuration 3, and d) configuration 4

Table 5 indicates the details of tri-objective optimization results comprising the optimum value of objectives and design parameters at the best point. The optimization results are obtained for the entire year, i.e., 8760 hours. According to the table, compared to the base case, a higher CDERR, ACSR, and PESR and lower purchased energy and the payback period is achieved at the best optimization point, disclosing the significance of tri-objective optimization. The table further shows that at the optimum condition, configuration 3 is the best model from a performance aspect due to the lowest purchased energy and higher PESR. Besides, it can be concluded that configuration 4, with the lowest total cost and payback period and highest ACSR, is the best, most favorable option from an economic viewpoint. In contrast, the table indicates that configuration 1, which is equipped with a battery, is the worst system from all facets due to the highest total cost and payback period and lowest ACSR, PESR, and CDERR.

Table 5. Tri-objective optimization results for each configuration.

| **Optimum parameters** | **Configuration 1** | **Configuration 2** | **Configuration 3** | **Configuration 4** |
|---|---|---|---|---|
| **Panel area ($m^2$)** | 17.1 | 16.3 | 15.9 | 15.6 |
| **Heat storage capacity (kWh)** | 543.4 | 538.3 | 393.3 | 459.5 |
| **Heat storage volume ($m^3$)** | 7.8 | 7.7 | 5.6 | 6.6 |
| **Cold storage (or battery*) capacity (kWh)** | 118.8* | 219.6 | 201.1 | 212.3 |
| **Cold storage (or battery*) volume ($m^3$)** | 0.3* | 3.1 | 2.8 | 3.1 |
| **PESR (%)** | 53.7 | 63.2 | 91.5 | 78.9 |
| **ACSR (%)** | 95.6 | 97.5 | 100.4 | 100.9 |
| **PP (year)** | 8.9 | 6.1 | 6.8 | 6.1 |
| **Total cost ($)** | 717696 | 596400 | 661360 | 590160 |
| **CDERR (%)** | 69.5 | 95.2 | 128.6 | 112.7 |
| **Purchased Energy (MWh)** | 415.5 | 472.6 | 170.9 | 318.5 |

## 5. Conclusions

In this study, the feasibility of a novel smart energy building system with the maximum possible energy efficiency, reliability, and cost-effectiveness for the building proprietors and the energy suppliers is studied. The target is achieved by eliminating the battery and minimizing the heat pump capacity, proposing the two-way interaction of the building with energy networks, replacing the PVT panel with PVTC, and using large-enough cold/heat storage units. For proving the proposed solution's proficiency, three more configurations as the most serious competitors of that (mainly those driven either by PVTC or PVT panels and interacting with the electricity grid and district heating and cooling (if any) networks) are considered for techno-economic benchmarking. The analysis and comparisons are made, taking Danish energy system rules, prices, and regulations for a 60-flat complex building as a case study. MATLAB software is applied to model and compare the performance of all the configurations from techno-economic-environmental aspects. Multi-objective optimization based on a genetic algorithm approach is applied to each configuration to find their best operating condition. The influence of significant decision parameters comprising panel area, heat, and cold storage tanks, and battery capacities on the performance of each configuration is examined and compared by evaluating their impact on the required external support, primary energy saving ratio, total cost, annual cost-saving ratio, payback period, and carbon dioxide emission reduction ratio. In summary, the main conclusions of the present work are as follow:

- The proposed solution (configuration 4, the one driven by PVTC with an innovative method of using heat pumps) is the best option among all due to its very short payback period of 6.3 years and higher primary energy saving rate and carbon dioxide emission reduction rate of 16.6% and 21.6%, compared to configuration 2.
- Totally removing the heat pump from this configuration (reaching configuration 2) would make the system very slightly more cost-effective (6.2 years of payback duration instead of 6.3 years) but less resilient/ and self-sufficient. In this case, if there is no access to an immediate auxiliary source or district heating/cooling network, the system would absolutely fail in covering the thermal energy demand of the end-users.
- Configuration 1, driven by PVT, has the lowest sold energy, primary energy saving, and carbon dioxide emission reduction rate compared to the other configurations equipped with PVTC, indicating the excellence of multi-generation electricity, heat, and cooling.
- The worst option from the economic facet is configuration 1, which is integrated with battery due to the highest total cost, annual cost-saving rate, and the payback period of 784,944 $, 87.3%, and 9.3 years, respectively.

- Configuration 3, equipped with a heat pump, is the best model from a performance aspect because of the highest primary energy saving and lowest purchased energy from the networks. However, it is not economically favorable due to the higher total cost and the payback period of 96,914.2 $, 71,039.2 $, 0.7 years, and 0.6 years compared to configuration 2 and configuration 4.
- At the tri-objective optimization point, while the carbon dioxide emission reduction rate, primary energy saving ratio, and annual cost-saving ratio of each configuration increase, the purchased energy and payback period decrease compared to the design condition.

## Appendix A. Normalized Pareto diagram

Normalized Pareto frontier diagram of net purchased energy from the networks, CDERR, and total cost for each configuration are presented in Figure A1 to find the best point among all the optimum points.

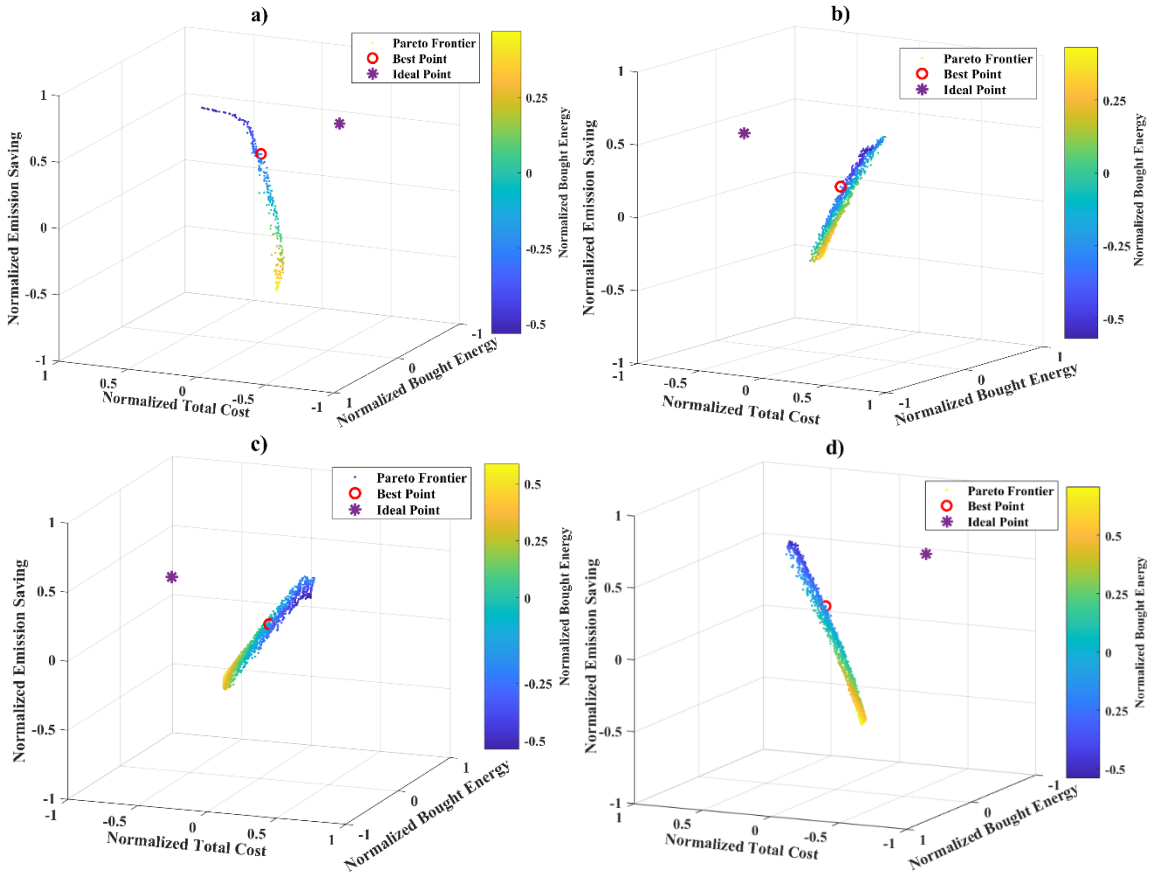


Figure A1. Normalized Pareto frontier diagram of carbon dioxide emission reduction rate, purchased energy, and total cost for a) configuration 1, b) configuration 2, c) configuration 3, and d) configuration 4

## Appendix B. Scatter distribution

Scatter distribution is demonstrated in Figure B to illustrate better each configuration's optimum domain of significant decision parameters. The figure indicates that the panel area and heat storage capacity are not

sensitive parameters since all of the optimal points are dispersed in the whole domain. From the figure, it can be further concluded that the optimum points of cold storage capacity are dispersed between 200 MWh and 400 MWh, where more points are close to the lower bound, i.e., 200 MWh.

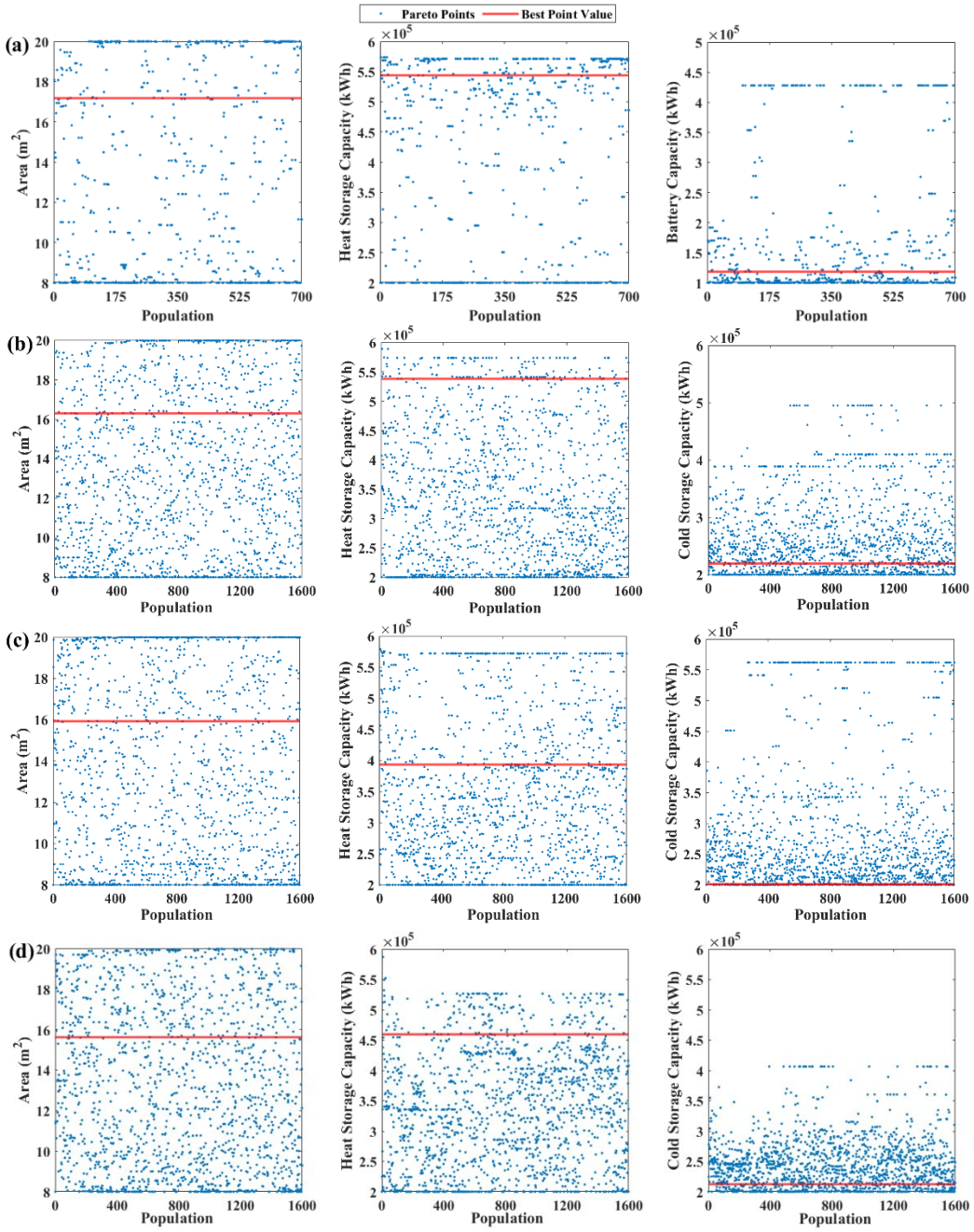


Figure B1. Scatter distribution of main design parameters of a) configuration 1, b) configuration 2, c) configuration 3, and d) configuration 4.

## Reference


[1] Bagherian MA, Mehranzamir K. A comprehensive review on renewable energy integration for combined heat and power production. Energy Convers Manag 2020;224:113454. doi:https://doi.org/10.1016/j.enconman.2020.113454.

[2] Azaza M, Eriksson D, Wallin F. A study on the viability of an on-site combined heat- and power supply system with and without electricity storage for office building. Energy Convers Manag 2020;213:112807. doi:https://doi.org/10.1016/j.enconman.2020.112807.

[3] Santamouris M. Innovating to zero the building sector in Europe: Minimising the energy consumption, eradication of the energy poverty and mitigating the local climate change. Sol Energy 2016;128:61–94. doi:https://doi.org/10.1016/j.solener.2016.01.021.

[4] Li H, Hou J, Hong T, Ding Y, Nord N. Energy, economic, and environmental analysis of integration of thermal energy storage into district heating systems using waste heat from data centres. Energy 2021;219:119582. doi:https://doi.org/10.1016/j.energy.2020.119582.

[5] Ifaei P, Karbassi A, Lee S, Yoo C. A renewable energies-assisted sustainable development plan for Iran using techno-econo-socio-environmental multivariate analysis and big data. Energy Convers Manag 2017;153:257–77. doi:https://doi.org/10.1016/j.enconman.2017.10.014.

[6] Gholamian E, Hanafizadeh P, Ahmadi P, Mazzarella L. A transient optimization and techno-economic assessment of a building integrated combined cooling, heating and power system in Tehran. Energy Convers Manag 2020;217:112962. doi:10.1016/J.ENCONMAN.2020.112962.

[7] Gorjian S, Calise F, Kant K, Ahamed MS, Copertaro B, Najafi G, et al. A review on opportunities for implementation of solar energy technologies in agricultural greenhouses. J Clean Prod 2021;285:124807. doi:https://doi.org/10.1016/j.jclepro.2020.124807.

[8] Behzadi A, Habibollahzade A, Ahmadi P, Gholamian E, Houshfar E. Multi-objective design optimization of a solar based system for electricity, cooling, and hydrogen production. Energy 2019;169. doi:10.1016/j.energy.2018.12.047.

[9] Good C, Andresen I, Hestnes AG. Solar energy for net zero energy buildings - A comparison between solar thermal, PV and photovoltaic-thermal (PV/T) systems. Sol Energy 2015;122:986–96. doi:10.1016/j.solener.2015.10.013.

[10] Conti P, Schito E, Testi D. Cost-benefit analysis of hybrid photovoltaic/thermal collectors in a nearly zero-energy building. Energies 2019;12. doi:10.3390/en12081582.

[11] Tse K, Chow T, Su Y. Performance evaluation and economic analysis of a full scale water-based photovoltaic / thermal ( PV / T ) system in an office building. Energy Build 2016;122:42–52. doi:10.1016/j.enbuild.2016.04.014.

[12] Wang K, Herrando M, Pantaleo AM, Markides CN. Technoeconomic assessments of hybrid photovoltaic-thermal vs. conventional solar-energy systems: Case studies in heat and power provision to sports centres. Appl Energy 2019;254:113657. doi:10.1016/j.apenergy.2019.113657.

[13] Kamel MA, Elbanhawy AY, Abo El-Nasr M. A novel methodology to compare between side-by-side photovoltaics and thermal collectors against hybrid photovoltaic thermal collectors. Energy Convers Manag 2019;202:112196. doi:10.1016/j.enconman.2019.112196.

[14] Herrando M, Ramos A, Zabalza I. Cost competitiveness of a novel PVT-based solar combined heating and power system: Influence of economic parameters and financial incentives. Energy Convers Manag 2018;166:758–70. doi:10.1016/j.enconman.2018.04.005.

[15] Ren F, Wei Z, Zhai X. Multi-objective optimization and evaluation of hybrid CCHP systems for different building types. Energy 2021;215:119096. doi:10.1016/j.energy.2020.119096.

[16] Arabkoohsar A, Alsagri AS. A new generation of district heating system with neighborhood-scale heat pumps and advanced pipes, a solution for future renewable-based energy systems. Energy 2020;193. doi:10.1016/j.energy.2019.116781.

[17] Zhang S, Zhuang Z, Hu Y, Yang B, Tan H. Applicability study on a hybrid renewable energy system for net-zero energy house in Shanghai. Energy Procedia 2016;88:768–74. doi:10.1016/j.egypro.2016.06.108.

[18] Gholamian E, Ahmadi P, Hanafizadeh P, Ashjaee M. Dynamic feasibility assessment and 3E analysis of a smart building energy system integrated with hybrid photovoltaic-thermal panels and energy storage. Sustain Energy Technol Assessments 2020;42:100835. doi:10.1016/j.seta.2020.100835.

[19] Del Amo A, Martínez-Gracia A, Pintanel T, Bayod-Rújula AA, Torné S. Analysis and optimization of a heat pump system coupled to an installation of PVT panels and a seasonal storage tank on an educational building. Energy Build 2020;226:110373. doi:10.1016/j.enbuild.2020.110373.

[20] Buonomano A, Calise F, Palombo A, Vicidomini M. Adsorption chiller operation by recovering low-temperature heat from building integrated photovoltaic thermal collectors : Modelling and

simulation. Energy Convers Manag 2017. doi:10.1016/j.enconman.2017.05.005.

[21] Pardo García N, Zubi G, Pasaoglu G, Dufo-López R. Photovoltaic thermal hybrid solar collector and district heating configurations for a Central European multi-family house. Energy Convers Manag 2017;148:915–24. doi:10.1016/j.enconman.2017.05.065.

[22] Behzadi A, Arabkoohsar A. Feasibility study of a smart building energy system comprising solar PV/T panels and a heat storage unit. Energy 2020:118528. doi:https://doi.org/10.1016/j.energy.2020.118528.

[23] Razmi AR, Arabkoohsar A, Nami H. Thermoeconomic analysis and multi-objective optimization of a novel hybrid absorption/recompression refrigeration system. Energy 2020;210:118559. doi:10.1016/j.energy.2020.118559.

[24] Rabani M, Bayera Madessa H, Nord N. Achieving zero-energy building performance with thermal and visual comfort enhancement through optimization of fenestration, envelope, shading device, and energy supply system. Sustain Energy Technol Assessments 2021;44:101020. doi:https://doi.org/10.1016/j.seta.2021.101020.

[25] Dannemand M, Perers B, Furbo S. Performance of a demonstration solar PVT assisted heat pump system with cold buffer storage and domestic hot water storage tanks. Energy Build 2019;188–189:46–57. doi:10.1016/j.enbuild.2018.12.042.

[26] Hazami M, Riahi A, Mehdaoui F, Nouicer O, Farhat A. Energetic and exergetic performances analysis of a PV/T (photovoltaic thermal) solar system tested and simulated under to Tunisian (North Africa) climatic conditions. Energy 2016;107:78–94. doi:10.1016/j.energy.2016.03.134.

[27] Chen JF, Zhang L, Dai YJ. Performance analysis and multi-objective optimization of a hybrid photovoltaic/thermal collector for domestic hot water application. Energy 2018;143:500–16. doi:10.1016/j.energy.2017.10.143.

[28] Sakellariou EI, Wright AJ, Axaopoulos P, Oyinlola MA. PVT based solar assisted ground source heat pump system: Modelling approach and sensitivity analyses. Sol Energy 2019;193:37–50. doi:10.1016/j.solener.2019.09.044.

[29] Behzadi A, Arabkoohsar A, Yang Y. Optimization and dynamic techno-economic analysis of a novel PVT-based smart building energy system. Appl Therm Eng 2020:115926. doi:https://doi.org/10.1016/j.applthermaleng.2020.115926.

[30] Fakhari I, Behzadi A, Gholamian E, Ahmadi P, Arabkoohsar A. Comparative double and integer

optimization of low-grade heat recovery from PEM fuel cells employing an organic Rankine cycle with zeotropic mixtures. Energy Convers Manag 2021;228:113695. doi:10.1016/j.enconman.2020.113695.

[31] KLEIN, A. S. TRNSYS-A transient system simulation program. Univ Wisconsin-Madison, Eng Exp Stn Rep 1988:38–12.

[32] Behzadi A, Arabkoohsar A. Comparative performance assessment of a novel cogeneration solar-driven building energy system integrating with various district heating designs. Energy Convers Manag 2020;220:113101. doi:10.1016/j.enconman.2020.113101.

[33] Jonas D, Lämmle M, Theis D, Schneider S, Frey G. Performance modeling of PVT collectors: Implementation, validation and parameter identification approach using TRNSYS. Sol Energy 2019;193:51–64. doi:https://doi.org/10.1016/j.solener.2019.09.047.

[34] Kalogirou SA. Chapter 5 - Solar Water-Heating Systems. In: Kalogirou SA, editor. Sol. Energy Eng. (Second Ed. Second Edi, Boston: Academic Press; 2014, p. 257–321. doi:https://doi.org/10.1016/B978-0-12-397270-5.00005-4.

[35] Anderson T, Duke M, Carson J. Performance of an unglazed solar collector for radiant cooling. Aust Sol Cool 2013.

[36] Duffie JA, Beckman WA. Wiley: Solar Engineering of Thermal Processes, 4th Edition - John A. Duffie, William A. Beckman. 2013.

[37] Dobson RT. Thermal modelling of a night sky radiation cooling system. J Energy South Africa 2005;16:20–31. doi:10.17159/2413-3051/2005/v16i2a3184.

[38] Sadi M, Chakravarty KH, Behzadi A, Arabkoohsar A. Techno-economic-environmental investigation of various biomass types and innovative biomass-firing technologies for cost-effective cooling in India. Energy 2021;219:119561. doi:https://doi.org/10.1016/j.energy.2020.119561.

[39] COWI - Powering your 360° solutions n.d. https://www.cowi.com/ (accessed January 10, 2021).

[40] Lithium Battery Management Systems (BMS) | LiTHIUM BALANCE n.d. https://lithiumbalance.com/ (accessed January 10, 2021).

[41] RACELL – Customised Solar Cells for Architecture n.d. http://racell.dk/ (accessed January 10, 2021).